

Revealing the Power of Masked Autoencoders in Traffic Forecasting

Jiarui Sun*
University of Illinois Urbana-Champaign
Urbana, IL, USA
jsun57@illinois.edu

Yujie Fan
Visa Research
Foster City, CA, USA
yufan@visa.com

Chin-Chia Michael Yeh
Visa Research
Foster City, CA, USA
miyeh@visa.com

Wei Zhang
Visa Research
Foster City, CA, USA
wzhan@visa.com

Girish Chowdhary
University of Illinois Urbana-Champaign
Urbana, IL, USA
girishc@illinois.edu

ABSTRACT

Traffic forecasting, crucial for urban planning, requires accurate predictions of spatial-temporal traffic patterns across urban areas. Existing research mainly focuses on designing complex models that capture spatial-temporal dependencies among variables explicitly. However, this field faces challenges related to data scarcity and model stability, which results in limited performance improvement. To address these issues, we propose Spatial-Temporal Masked AutoEncoders (STMAE), a plug-and-play framework designed to enhance existing spatial-temporal models on traffic prediction. STMAE consists of two learning stages. In the pretraining stage, an encoder processes partially visible traffic data produced by a dual-masking strategy, including biased random walk-based spatial masking and patch-based temporal masking. Subsequently, two decoders aim to reconstruct the masked counterparts from both spatial and temporal perspectives. The fine-tuning stage retains the pretrained encoder and integrates it with decoders from existing backbones to improve forecasting accuracy. Our results on traffic benchmarks show that STMAE can largely enhance the forecasting capabilities of various spatial-temporal models.

CCS CONCEPTS

• **Computing methodologies** → **Neural networks.**

KEYWORDS

Masked autoencoders; Spatial-temporal models; Traffic forecasting

ACM Reference Format:

Jiarui Sun, Yujie Fan, Chin-Chia Michael Yeh, Wei Zhang, and Girish Chowdhary. 2024. Revealing the Power of Masked Autoencoders in Traffic Forecasting. In *Proceedings of the 33rd ACM International Conference on Information and Knowledge Management (CIKM '24)*, October 21–25, 2024, Boise, ID, USA. ACM, New York, NY, USA, 10 pages. <https://doi.org/10.1145/3627673.3679989>

*Work done while at Visa Research. Our code is released at: <https://github.com/jsun57/STMAE>.

Permission to make digital or hard copies of all or part of this work for personal or classroom use is granted without fee provided that copies are not made or distributed for profit or commercial advantage and that copies bear this notice and the full citation on the first page. Copyrights for third-party components of this work must be honored. For all other uses, contact the owner/author(s).
CIKM '24, October 21–25, 2024, Boise, ID, USA
© 2024 Copyright held by the owner/author(s).
ACM ISBN 979-8-4007-0436-9/24/10
<https://doi.org/10.1145/3627673.3679989>

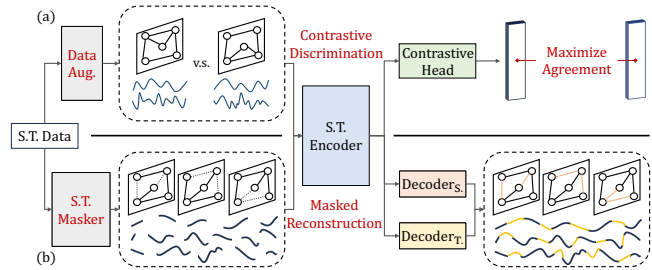


Figure 1: Illustration of SSL approaches: (a) Contrastive-based and (b) Mask-based frameworks for traffic forecasting.

1 INTRODUCTION

Spatial-temporal forecasting is a pivotal task with applications in numerous fields, including human motion modeling [16, 20] and epidemic simulation [2, 10]. Within these applications, traffic forecasting emerges as a crucial area for urban planning and management. This particular aspect of spatial-temporal analysis focuses on predicting traffic flow and speed based on historical data, which is essential for optimizing transportation systems. To make accurate predictions, state-of-the-art methods develop spatial-temporal models to capture complex interactions of traffic data over both space and time. By jointly modeling spatial and temporal patterns, these models exhibit remarkable traffic prediction performance.

However, despite efforts, several issues impede the performance of spatial-temporal models. First, *data scarcity* in traffic datasets often leads to *model overfitting*. Unlike domains such as computer vision which utilize massive datasets for training, traffic benchmarks typically cover only a few months and are limited to specific geographic locations. This constrained data scope makes it difficult for models to generalize well across varying traffic patterns, increasing the risk of overfitting. Second, *data incompleteness* poses challenges to *model stability*. Traffic data, collected from sensors deployed across road networks, inevitably suffer from inconsistencies due to sensor malfunctions. These issues lead to gaps and errors in the data, resulting in unstable training conditions for spatial-temporal models, which ultimately compromises their performance.

Self-supervised learning (SSL) [29] offers a promising avenue for mitigating the above challenges. Contrastive SSL, for instance, shows potential by learning to contrast sample pairs, as depicted

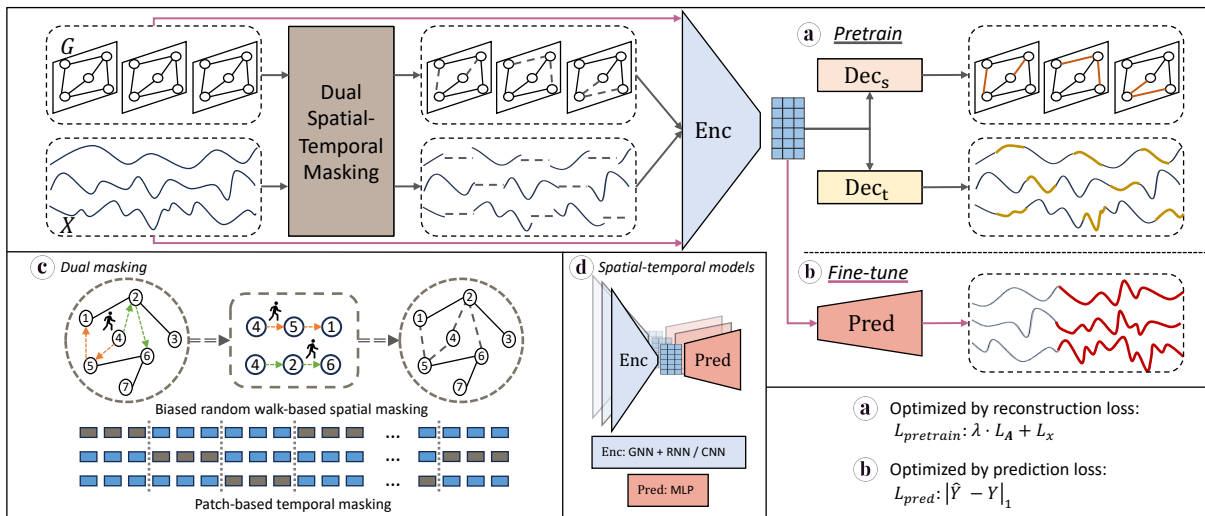


Figure 2: The STMAE framework, including the (a) pretraining and (b) fine-tuning stages. Specified by (c), We use a biased random walk-based spatial masking strategy on G , and a patch-based temporal masking strategy on X . After reconstruction, learning is guided jointly by \mathcal{L}_A and \mathcal{L}_X . As shown in (d), STMAE can be easily plugged into existing spatial-temporal models.

in fig. 1 (a). However, this method heavily depends on manually crafted heuristics to derive data samples, which are limited in the traffic scenario. To overcome the limitation, we turn to generative SSL [15], specifically Masked Autoencoders (MAE) [8] as a more potent solution. Illustrated in fig. 1 (b), MAE focuses on reconstructing masked portions of input data to learn robust features, and can be seamlessly integrated to spatial-temporal models for traffic forecasting. Notably, this approach not only mitigates overfitting via self-reconstruction but also improves model stability by learning from incomplete data, thus enhancing prediction accuracy.

Inspired by MAE, we present *Spatial-Temporal Masked AutoEncoders* (STMAE), a versatile framework that leverages the principles of MAE to elevate the capability of existing spatial-temporal models for traffic forecasting. STMAE, shown in Figure 2, includes pretraining and fine-tuning stages. Initially, an encoder from an existing spatial-temporal model, along with two decoders, reconstructs masked traffic data produced by a *dual-masking strategy* that combines biased random walk-based spatial and patch-based temporal masking. This challenges the encoder to acquire robust and predictive traffic features. In the fine-tuning phase, the encoder is retained, and the decoders are replaced with the original predictor from the backbone for forecasting. STMAE offers seamless integration to existing models without needing complex data augmentation, positioning itself as a flexible and powerful enhancement tool for traffic forecasting. Our primary contributions are summarized below:

- We present STMAE, a versatile framework that seamlessly integrates with established spatial-temporal backbones, alleviating model overfitting and stability concerns.
- We propose a dual-masking strategy, including biased random walk-based spatial masking and patch-based temporal masking. This establishes a challenging pretext task that encourages the encoder to acquire informative traffic data representations.

- We conducted extensive experiments on various traffic benchmarks, showing large performance enhancements over existing spatial-temporal models.

2 RELATED WORK

2.1 Spatial-Temporal Models

By considering the interdependence among different variables, spatial-temporal models [4, 11, 25, 28, 30] have shown remarkable traffic forecasting performance. For example, Li *et al.* introduced DCRNN [13], which utilizes RNN-based graph diffusion convolution to capture spatial-temporal correlations. Bai *et al.* proposed AGCRN [1], which incorporates several adaptive graph learning modules that dynamically capture sensor dependencies recurrently. Wu *et al.* designed MTGNN [24], which learns spatial-temporal correlations among traffic sensors effectively using adaptive GNN and CNN-based modules. Despite these innovations, the limited scale of traffic data often leads to model overfitting. Addressing these challenges, Liu *et al.* introduced STGCL [14], using contrastive SSL to enhance model learning from traffic network structures and temporal patterns. However, STGCL's reliance on specific data knowledge limits its application. In contrast, our STMAE framework provides a flexible, plug-and-play solution without needing such detailed prior information, offering a robust enhancement to existing models.

2.2 Masked Autoencoders

Masked autoencoders (MAE) are a generative SSL method for robust feature representation learning [3, 5, 8]. MAE employs an encoder to map masked inputs to latent representations and a decoder for reconstruction. It has been adapted across domains: BERT [3] uses bidirectional context to model language through sentence masking, while the visual MAE [8] is designed for image learning. MAE has also been applied to graphs [9, 12, 22, 23, 26]. These methods underscore its potential as a unified representation learning method

with minimal domain knowledge. On a similar line of our work, STEP [17] uses a feature masking strategy with a Transformer model to encode temporal patterns from long-term traffic data. Contrary to STEP with its specialized architecture, STMAE is a more generalizable enhancer for various spatial-temporal backbones.

3 PRELIMINARIES

3.1 Traffic Forecasting

Given traffic data $\mathcal{X} \in \mathbb{R}^{H \times N \times C}$ with H frames of N variables and C features, traffic forecasting predicts future traffic $\hat{\mathcal{Y}} \in \mathbb{R}^{F \times N \times C}$ for F steps. The variables in \mathcal{X} are spatially interrelated, represented by a graph $\mathcal{G} = (\mathcal{V}, \mathcal{E}, \mathbf{A})$, with $\mathbf{A} \in \mathbb{R}^{N \times N}$ as the adjacency matrix representing connectivity. The forecasting problem can be defined as $f_\theta(\mathcal{X}, \mathbf{A}) \rightarrow \hat{\mathcal{Y}}$, where $f_\theta(\cdot)$ is the parameterized forecaster.

3.2 Pipeline of Spatial-Temporal Models

Existing spatial-temporal models often employ an encoder-decoder design. The *encoder*, $\text{Enc}(\mathcal{X}, \mathbf{A}) \rightarrow \mathbf{S}$, extracts complex spatial-temporal patterns from historical data into a hidden representation $\mathbf{S} \in \mathbb{R}^{N \times D}$, where D is the hidden dimension. On the other hand, the *predictor* (decoder), denoted as $\text{Pred}(\mathbf{S}) \rightarrow \hat{\mathcal{Y}}$, focuses on making predictions based on the encoded state \mathbf{S} . In contrast to the encoder, $\text{Pred}(\cdot)$ is typically lightweight, often designed as a multi-layer perceptron (MLP) with few layers. Therefore, the pipeline of spatial-temporal models for traffic forecasting can be summarized as: $f_\theta(\mathcal{X}, \mathbf{A}) := \text{Pred}(\text{Enc}(\mathcal{X}, \mathbf{A})) \rightarrow \hat{\mathcal{Y}}$. Lastly, the mean absolute error between predictions $\hat{\mathcal{Y}}$ and groundtruth \mathcal{Y} is used as the objective to train spatial-temporal models. This forecasting loss can be represented as $\mathcal{L}_{\text{pred}} = \|\hat{\mathcal{Y}} - \mathcal{Y}\|_1$.

4 METHODOLOGY

STMAE implements a two-stage training process: pretraining and fine-tuning. During pretraining, STMAE reconstructs masked traffic data using dual spatial-temporal masking. The fine-tuning stage utilizes the pretrained encoder to generate contextual representations for the predictor. STMAE adopts existing spatial-temporal model components for both the encoder and predictor.

4.1 Pretraining

The pretraining stage uncovers spatial-temporal patterns in traffic data via self-supervised masking. First, we enhance existing encoders $\text{Enc}(\cdot)$ with a dual masking module. Given the spatial-temporal interactions in traffic data, we combine spatial and temporal masking rather than isolating one domain. For the masking approach, spatially, we use biased random walk-based masking instead of simple uniform masking to preserve and challenge structural integrity of traffic networks. Temporally, we employ patch-based masking, dividing data into non-overlapping patches and masking these, which proves more challenging than masking single timesteps. Each component is detailed below.

Spatial Masking. While existing graph MAEs often uniformly mask a subset of relations, we enhance the challenge by using paths as the basic unit of masking to capture more complex structures. Leveraging a *biased random walk-based spatial masking* strategy inspired by [6], we generate paths using a biased random walker

that blends breadth-first and depth-first sampling, enabling deeper graph exploration. Relations for masking $\mathcal{E}_{\text{mask}}$ with size $|\mathcal{E}| \cdot p_s$ are selected from \mathcal{E} as:

$$\mathcal{E}_{\text{mask}} \sim \text{BiasedRandomWalk}(\mathcal{E}, \mathcal{R}, p, q), \quad (1)$$

where p_s is the spatial masking ratio, $\mathcal{R} \in \mathcal{V}$ is the set of root nodes, and p and q are hyperparameters controlling the walk dynamics. Masked relations are then set to zero in the adjacency matrix \mathbf{A} :

$$\mathbf{A}_{uv} \leftarrow \begin{cases} 0 & (u, v) \in \mathcal{E}_{\text{mask}}, \\ \mathbf{A}_{uv} & \text{otherwise.} \end{cases} \quad (2)$$

Our spatial masking strategy enhances the reconstruction task's complexity and the encoder's capacity to infer hidden structure.

Temporal Masking. With relatively low information density, traffic data can be easily recovered by interpolation, especially when temporal masking areas are sparse. To counteract this, we implement *patch-based temporal masking*. We partition the original data \mathcal{X} into P nonoverlapping temporal patches, each of length L , and selectively mask a subset of these patches. Masked patches are then substituted with a shared, learnable mask token. Let $\{\mathcal{X}_i\}_{i=1}^P$ represent the embedding patches with $\mathcal{X}_i \in \mathbb{R}^{L \times N \times D}$. Temporal masking is defined as:

$$\mathcal{X}_i \leftarrow \begin{cases} \mathcal{M} & r \sim \text{Bernoulli}(p_t), r = 1, \\ \mathcal{X}_i, & \text{otherwise,} \end{cases} \quad (3)$$

where \mathcal{M} is the mask token and p_t is the temporal masking ratio.

Decoders. Second, two lightweight decoders are used for reconstruction. The decoders' goal is to reconstruct both \mathbf{A} and \mathcal{X} simultaneously. After masking, the masked inputs \mathbf{A}_M and \mathcal{X}_M are encoded by $\text{Enc}(\cdot)$ into a state \mathbf{S} . Now, instead of predicting $\hat{\mathcal{Y}}$ directly, the goal is to reconstruct the original inputs from both spatial and temporal dimensions using two specialized decoders: $\text{Dec}_t(\cdot)$ for data and $\text{Dec}_s(\cdot)$ for structural dependencies:

$$\mathbf{S} = \text{Enc}(\mathcal{X}_M, \mathbf{A}_M), \hat{\mathcal{X}} = \text{Dec}_t(\mathbf{S}), \hat{\mathbf{A}} = \text{Dec}_s(\mathbf{S}), \quad (4)$$

where $\hat{\mathcal{X}}$ and $\hat{\mathbf{A}}$ are the reconstructed data and adjacency matrix. The spatial decoder, $\text{Dec}_s(\cdot)$, performs a linear transformation followed by a sigmoid operation:

$$\hat{\mathbf{A}}_{uv} = \text{Sigmoid}((\mathbf{S}\mathbf{W})(\mathbf{S}\mathbf{W})^T uv), \quad (5)$$

with $\mathbf{W} \in \mathbb{R}^{D \times D}$ as a trainable matrix. The temporal decoder, $\text{Dec}_t(\cdot)$, uses a linear layer to map \mathbf{S} back to its original dimensions. This asymmetric encoder-decoder setup is designed to maximize the encoder's ability to capture detailed spatial-temporal interactions.

Reconstruction Targets. To guide spatial-temporal reconstruction, we leverage two objectives, consisting of a classification loss \mathcal{L}_A and a regression loss \mathcal{L}_X tailored to adjacency matrix \mathbf{A} and the data \mathcal{X} , respectively. Specifically, \mathcal{L}_A aims to reconstruct the masked walks using a classification objective. Formally, we have:

$$\mathcal{L}_A = -\frac{1}{|\mathcal{E}_{\text{mask}}|} \sum_{(u,v) \in \mathcal{E}_{\text{mask}}} \log \hat{\mathbf{A}}_{uv}. \quad (6)$$

On the other hand, \mathcal{L}_X computes the mean absolute error of the masked patches between \mathcal{X} and the reconstruction $\hat{\mathcal{X}}$:

$$\mathcal{L}_X = \|\hat{\mathcal{X}}_{[M]} - \mathcal{X}_{[M]}\|_1, \quad (7)$$

Table 1: Quantitative results of STMAE compared with STGCL and various base models. Subscripts A, D, M correspond to the initials of the base models in which STMAE and STGCL are coupled with.

Datasets	PEMS03			PEMS04			PEMS07			PEMS08		
	MAE	MAPE	RMSE	MAE	MAPE	RMSE	MAE	MAPE	RMSE	MAE	MAPE	RMSE
AGCRN [1]	15.47	15.26	27.06	19.39	13.24	31.07	20.64	8.80	34.19	15.65	10.33	24.51
STGCL _A	15.36	14.85	27.15	19.23	13.01	31.36	20.61	8.74	34.14	15.91	10.43	24.88
STMAE _A	15.09	14.72	26.61	19.05	12.91	31.32	20.13	8.53	33.79	15.01	9.79	23.97
DCRNN [13]	15.76	15.69	26.76	21.48	14.65	33.99	22.55	9.78	35.24	16.63	10.78	26.01
footnotesizeSTGCL _D	15.64	15.68	27.08	21.23	14.57	33.60	22.34	9.68	35.21	16.51	10.70	25.93
STMAE _D	15.74	15.44	26.73	21.20	14.23	33.57	22.12	9.45	34.98	16.36	10.68	25.76
MTGNN [24]	14.94	16.02	25.29	19.02	13.32	30.95	20.83	9.00	33.77	15.44	10.35	24.30
STGCL _M	14.87	15.37	25.53	18.94	13.34	30.79	20.72	8.95	33.78	15.39	10.13	24.32
STMAE _M	14.84	14.15	24.95	18.87	12.78	30.28	20.57	8.90	33.47	15.03	9.82	24.08

where the subscript $[M]$ denotes the masked area index. In line with recent work [21], we only compute losses over the masked portions. The overall objective of the pretraining stage is:

$$\mathcal{L}_{\text{pretrain}} = \lambda \cdot \mathcal{L}_A + \mathcal{L}_X, \quad (8)$$

where λ is a non-negative hyperparameter trading off the spatial reconstruction loss and the temporal reconstruction loss.

4.2 Fine-tuning

After pretraining the encoder $\text{Enc}(\cdot)$ with the reconstruction objectives, we fine-tune $\text{Enc}(\cdot)$ with the original predictor $\text{Pred}(\cdot)$ obtained from spatial-temporal models to predict \hat{Y} . In this stage, we provide $\text{Enc}(\cdot)$ with the complete spatial-temporal data without masking, as opposed to the pretraining stage and discard the spatial decoder $\text{Dec}_s(\cdot)$ and the temporal decoder $\text{Dec}_t(\cdot)$. This fine-tuning process aligns with the training pipeline described in section 3.2, aiming to optimize the forecasting loss $\mathcal{L}_{\text{pred}}$.

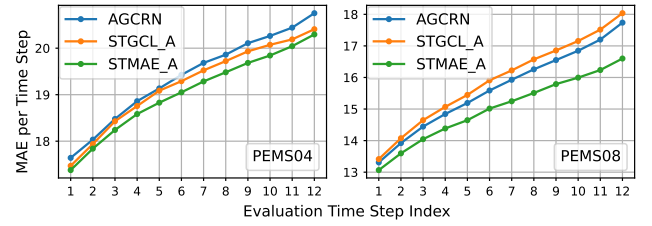
5 EXPERIMENTS

5.1 Experimental Setup

Datasets. Four traffic benchmarks—PEMS03, PEMS04, PEMS07, and PEMS08 [11, 14, 19]—are used to assess STMAE’s effectiveness. Each dataset is split into training, validation, and test sets in a 6:2:2 ratio chronologically. The training set supports both pretraining and fine-tuning phases, consistent with standard practices [27]. For a fair comparison with previous methods, we predict the next 12 steps based on 12-step historical traffic flow data.

Base Models and Metrics. STMAE is evaluated against STGCL [14], which uses contrastive SSL to enhance spatial-temporal models on traffic forecasting. Within STMAE, we incorporate widely recognized models DCRNN [13], AGCRN [1], and MTGNN [24] to assess their performance improvements with our approach. DCRNN requires a predefined graph as input, whereas AGCRN and MTGNN dynamically learn the graph structure during training. We adopt three metrics, including mean absolute error (MAE), root mean squared error (RMSE), and mean absolute percentage error (MAPE).

Implementation Details. STMAE is a versatile framework that can be seamlessly integrated into existing spatial-temporal backbones, in which the encoder $\text{Enc}(\cdot)$ and the predictor $\text{Pred}(\cdot)$ are

**Figure 3: Per-step MAE results of STMAE_A compared with its corresponding base model AGCRN and STGCL_A.**

taken directly from the base models. Therefore, our framework avoids extensive hyper-parameter tuning, such as adjusting model depth, batch size, hidden dimension and learning rate, which are commonly practiced to obtain optimal results for spatial-temporal models. For hyper-parameters required for STMAE, we conduct a grid search to determine few hyper-parameters: L from $\{2, 3\}$, p , q , λ from $\{0.5, 1, 2, 4\}$ and the masking ratios from 20% to 80% based on the validation MAE performance. For all datasets, we pretrain STMAE for 100 epochs, followed by 100 epochs of fine-tuning.

5.2 Results

Quantitative Results. Table 1 summarizes the experimental results averaged across all evaluation timesteps on four datasets. Through analysing the results, we have the following observations: (1) Demonstrated by the comparison among three base models, AGCRN and MTGNN, that dynamically learn the graph from the data, tend to outperform DCRNN, which relies on a predefined graph. (2) SSL can enhance the capability of spatial-temporal models for the traffic forecasting task, as both STGCL and STMAE achieve better performance than the backbones at most scenarios. (3) Our proposed STMAE, which leverages generative-based SSL through masking reconstruction, always outperforms STGCL, which is contrastive learning-based. More importantly, it does not require complex data augmentation processes that STGCL heavily relies on. This shows the efficacy of our framework.

To gain a deeper insight into the predictive capabilities of STMAE, we illustrate the per-step MAE results of STMAE_A and its corresponding base model and STGCL_A in fig. 3. Upon analysing the

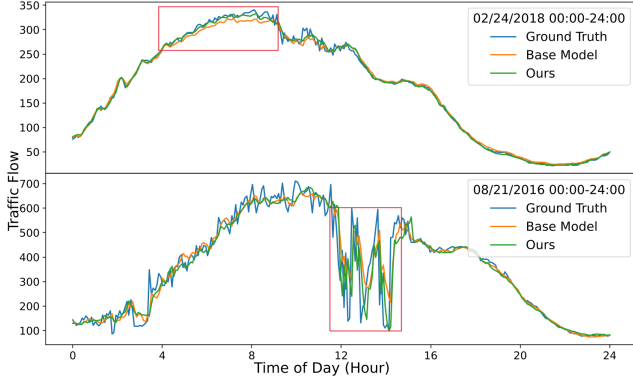


Figure 4: Visualization of one-hour-ahead predictions on two snapshots from PEMS04 and PEMS08 test sets.

results, we have the following conclusions: (1) The prediction error is positively correlated with the forecasting step as MAE continues to increase as the forecasting step becomes larger. This indicates the performance degradation issue of traffic forecasting. (2) STMAE_A consistently outperforms STGCL_A and their respective base models in terms of MAE at each timestep. (3) Importantly, as evaluation forecasting timestep increases, the performance gap between STMAE and the two variants gradually widens. This suggests that STMAE, aided by masked self-supervision, can effectively alleviate the performance degradation issue.

Qualitative Visualization. To study STMAE’s predictive ability qualitatively, we randomly select two sensors from PEMS04 and PEMS08, and visualize one-hour-ahead predictions of STMAE_A and AGCRN against the groundtruth on a test snapshot in fig. 4. We observe that STMAE outperforms the counterpart base model both in areas with gradual or sudden changes (red rectangles), showing STMAE’s efficacy in adapting to various spatial-temporal patterns.

5.3 Ablation Study

In STMAE, a dual-masking strategy is proposed for model pretraining, targeting both spatial and temporal dimensions. To assess this, we introduced three variants: STMAE_{NT} (no temporal masking), STMAE_{NS} (no spatial masking), and STMAE_U (uniform spatial-temporal masking). All ablation results are presented in table 2, with AGCRN serving as the backbone and PEMS04, PEMS08 as evaluation datasets. The experimental results yield the following insights: (1) Both STMAE_{NT} and STMAE_{NS} improve MAE performance, confirming the efficacy of individual spatial and temporal masking in the pretraining phase. (2) STMAE_U outperforms STMAE_{NT} and STMAE_{NS} in terms of MAE. This suggests that jointly applying masking techniques from both spatial and temporal perspectives is more advantageous for accurate prediction. (3) STMAE achieves superior performance compared to the base model and all its variants in terms of MAE, and it consistently ranks either first or second in terms of MAPE and RMSE metrics. This underscores the advantages of our approach, where the dual masking strategy can create challenging pretext tasks for spatial-temporal models, thus improving their traffic forecasting capacities.

Table 2: Ablations of STMAE_A on PEMS04 and PEMS08.

Variant	PEMS04			PEMS08		
	MAE	MAPE	RMSE	MAE	MAPE	RMSE
Base Model	19.39	13.24	31.07	15.65	10.33	24.51
STMAE _{NT}	19.27	13.32	31.07	15.41	10.08	24.26
STMAE _{NS}	19.27	12.85	31.34	15.26	9.89	24.43
STMAE _U	19.11	12.96	31.67	15.09	10.03	24.22
STMAE	19.05	12.91	31.32	15.01	9.79	23.97

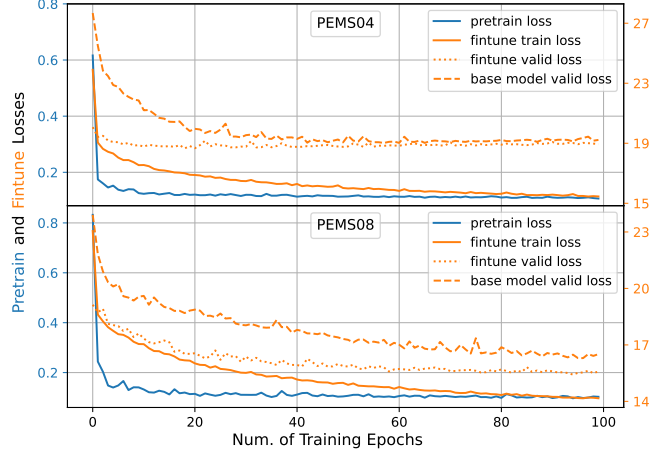


Figure 5: Training and validation processes of STMAE_A and AGCRN on PEMS04 and PEMS08. Both pretraining and fine-tuning are performed for 100 epochs.

5.4 Stability Study

This section investigates STMAE’s stability with an in-depth analysis of its learning behavior on PEMS04 and PEMS08 datasets. In Figure 5, we plot the learning curves for both the pretraining and fine-tuning stages of STMAE_A, alongside the learning curve for the AGCRN backbone. Our analysis of the plot leads us to the following conclusions: (1) Both the pretraining and fine-tuning stages of STMAE are stable, as both training curves of STMAE (*i.e.*, pretrain loss and fine-tune train loss) depict a smoothly decreasing trend. (2) The pretraining stage proves advantageous for STMAE. Specifically, for the PEMS04 dataset, STMAE exhibits a significantly lower initial validation loss compared to the base model, indicating a more effective starting point for fine-tuning. For the PEMS08 dataset, STMAE not only starts with a lower initial validation loss but also maintains this lead to achieve a substantially lower final validation loss. This underscores the effectiveness of the dual reconstruction objective employed during the pretraining phase, which enables STMAE to initialize more effectively. (3) In contrast to STMAE, the validation curves of the base model exhibit a more erratic fluctuation behavior with a higher MAE level. In summary, all three observations above signify the stability of STMAE.

5.5 Masking Ratio Sensitivity

In this section, we examine STMAE’s sensitivity to its key hyperparameters, *i.e.*, the spatial and temporal masking ratios. We explore the impact of varying these ratios from 20% to 80% when coupling STMAE with AGCRN. Test MAE results for PEMS04 and

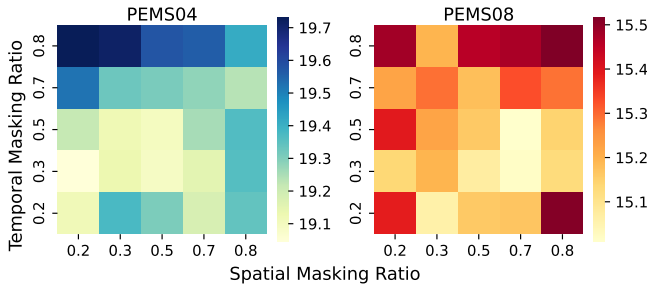


Figure 6: Masking ratio sensitivity analysis of STMAE_A on PEMS04 and PEMS08. Heatmaps show test MAE scores.

PEMS08 datasets are shown in fig. 6. The heatmaps indicate that STMAE achieves the best performance with a temporal masking ratio of 30% for both datasets. Spatially, it peaks at a 70% masking ratio for PEMS08 and 30% for PEMS04. We hypothesize that this difference is attributed to the greater structural density of PEMS08’s traffic network (0.01 for PEMS08 vs. 0.004 for PEMS04). Notably, STMAE underperforms when masking ratios are either too high or too low. This observation, in conjunction with our ablation study, underscores the efficacy of our dual masking strategy in enhancing spatial-temporal model performance in traffic forecasting.

6 CONCLUSION

Spatial-temporal models are effective for traffic forecasting but often face challenges related to overfitting and instability due to data scarcity and incompleteness. In response, we explore generative SSL and propose a novel framework STMAE based on masking reconstruction. STMAE integrates seamlessly into existing traffic forecasting spatial-temporal frameworks, structured around pre-training and fine-tuning phases. During pretraining, our novel dual masking strategy—utilizing biased random walk-based spatial and patch-based temporal masking—presents rigorous challenges that prompt the encoder to learn robust spatial-temporal patterns. In the fine-tuning stage, we leverage the pretrained encoder with the original predictor to improve forecast accuracy. Comprehensive evaluations on multiple traffic benchmarks affirm that STMAE greatly enhances the performance of traffic forecasting models. Ablation studies further validate the effectiveness of our dual-masking strategy in addressing the specific challenges of traffic prediction.

REFERENCES

- [1] Lei Bai, Lina Yao, Can Li, Xianzhi Wang, and Can Wang. 2020. Adaptive graph convolutional recurrent network for traffic forecasting. *Advances in neural information processing systems* 33 (2020), 17804–17815.
- [2] Songgaojun Deng, Shusen Wang, Huzefa Rangwala, Lijing Wang, and Yue Ning. 2020. Cola-GNN: Cross-location Attention based Graph Neural Networks for Long-term ILI Prediction. In *CIKM*. 245–254.
- [3] Jacob Devlin, Ming-Wei Chang, Kenton Lee, and Kristina Toutanova. 2019. BERT: Pre-training of Deep Bidirectional Transformers for Language Understanding. In *NAACL-HLT*. 4171–4186. <https://doi.org/10.18653/v1/n19-1423>
- [4] Zheng Fang, Qingqing Long, Guojie Song, and Kunqing Xie. 2021. Spatial-Temporal Graph ODE Networks for Traffic Flow Forecasting. In *KDD*. 364–373. <https://doi.org/10.1145/3447548.3467430>
- [5] Christoph Feichtenhofer, Yanghao Li, Kaiming He, et al. 2022. Masked autoencoders as spatiotemporal learners. *Advances in neural information processing systems* 35 (2022), 35946–35958.
- [6] Aditya Grover and Jure Leskovec. 2016. node2vec: Scalable Feature Learning for Networks. In *KDD*. 855–864. <https://doi.org/10.1145/2939672.2939754>
- [7] Shengnan Guo, Youfang Lin, Ning Feng, Chao Song, and Huaiyu Wan. 2019. Attention Based Spatial-Temporal Graph Convolutional Networks for Traffic Flow Forecasting. In *AAAI*. 922–929. <https://doi.org/10.1609/aaai.v33i01.3301922>
- [8] Kaiming He, Xinlei Chen, Saining Xie, Yanghao Li, Piotr Dollár, and Ross B. Girshick. 2022. Masked Autoencoders Are Scalable Vision Learners. In *CVPR*. 15979–15988. <https://doi.org/10.1109/CVPR52688.2022.01553>
- [9] Zhenyu Hou, Xiao Liu, Yukuo Cen, Yuxiao Dong, Hongxia Yang, Chunjie Wang, and Jie Tang. 2022. GraphMAE: Self-Supervised Masked Graph Autoencoders. In *KDD*. 594–604. <https://doi.org/10.1145/3534678.3539321>
- [10] Amol Kapoor, Xue Ben, Luyang Liu, Bryan Perozzi, Matt Barnes, Martin Blais, and Shawn O’Banion. 2020. Examining COVID-19 Forecasting using Spatio-Temporal Graph Neural Networks. *CoRR* abs/2007.03113 (2020). [arXiv:2007.03113](https://arxiv.org/abs/2007.03113) <https://arxiv.org/abs/2007.03113>
- [11] Shiyong Lan, Yitong Ma, Weikang Huang, Wenwu Wang, Hongyu Gan, and Pyang Li. 2022. DSTAGNN: Dynamic Spatial-Temporal Aware Graph Neural Network for Traffic Flow Forecasting. In *ICML*, Vol. 162. 11906–11917. <https://proceedings.mlr.press/v162/lan22a.html>
- [12] Jintang Li, Ruofan Wu, Wangbin Sun, Liang Chen, Sheng Tian, Liang Zhu, Changhua Meng, Zibin Zheng, and Weiqiang Wang. 2023. What’s Behind the Mask: Understanding Masked Graph Modeling for Graph Autoencoders. In *KDD*. 1268–1279. <https://doi.org/10.1145/3580305.3599546>
- [13] Yaguang Li, Rose Yu, Cyrus Shahabi, and Yan Liu. 2018. Diffusion Convolutional Recurrent Neural Network: Data-Driven Traffic Forecasting. In *ICLR*. <https://openreview.net/forum?id=SJIHXGWAZ>
- [14] Xu Liu, Yuxuan Liang, Chao Huang, Yu Zheng, Bryan Hooi, and Roger Zimmermann. 2022. When do contrastive learning signals help spatio-temporal graph forecasting?. In *SIGSPATIAL*. 5:1–5:12. <https://doi.org/10.1145/3557915.3560939>
- [15] Xiao Liu, Fanjin Zhang, Zhenyu Hou, Li Mian, Zhaoyu Wang, Jing Zhang, and Jie Tang. 2023. Self-Supervised Learning: Generative or Contrastive. *IEEE TKDE* 35, 1 (2023), 857–876. <https://doi.org/10.1109/TKDE.2021.3090866>
- [16] Wei Mao, Miaomiao Liu, Mathieu Salzmann, and Hongdong Li. 2019. Learning Trajectory Dependencies for Human Motion Prediction. In *ICCV*. IEEE, 9488–9496. <https://doi.org/10.1109/ICCV.2019.00958>
- [17] Zezhi Shao, Zhao Zhang, Fei Wang, and Yongjun Xu. 2022. Pre-training Enhanced Spatial-temporal Graph Neural Network for Multivariate Time Series Forecasting. In *KDD*. 1567–1577. <https://doi.org/10.1145/3534678.3539396>
- [18] David I. Shuman, Sunil K. Narang, Pascal Frossard, Antonio Ortega, and Pierre Vandergheynst. 2013. The Emerging Field of Signal Processing on Graphs: Extending High-Dimensional Data Analysis to Networks and Other Irregular Domains. *IEEE Signal Process. Mag.* 30, 3 (2013), 83–98.
- [19] Chao Song, Youfang Lin, Shengnan Guo, and Huaiyu Wan. 2020. Spatial-Temporal Synchronous Graph Convolutional Networks: A New Framework for Spatial-Temporal Network Data Forecasting. In *AAAI*. 914–921. <https://ojs.aaai.org/index.php/AAAI/article/view/5438>
- [20] Jiarui Sun and Girish Chowdhary. 2023. Towards Globally Consistent Stochastic Human Motion Prediction via Motion Diffusion. *CoRR* abs/2305.12554 (2023). <https://doi.org/10.48550/arXiv.2305.12554> [arXiv:2305.12554](https://arxiv.org/abs/2305.12554)
- [21] Qiaoyu Tan, Ninghao Liu, Xiao Huang, Rui Chen, Soo-Hyun Choi, and Xia Hu. 2022. MGAE: Masked Autoencoders for Self-Supervised Learning on Graphs. *CoRR* abs/2201.02534 (2022). <https://arxiv.org/abs/2201.02534>
- [22] Qiaoyu Tan, Ninghao Liu, Xiao Huang, Soo-Hyun Choi, Li Li, Rui Chen, and Xia Hu. 2023. S2GAE: Self-Supervised Graph Autoencoders are Generalizable Learners with Graph Masking. In *WSDM*. 787–795. <https://doi.org/10.1145/3539597.3570404>
- [23] Yijun Tian, Kaiwen Dong, Chunhui Zhang, Chuxu Zhang, and Nitesh V. Chawla. 2023. Heterogeneous Graph Masked Autoencoders. In *AAAI*. 9997–10005. <https://doi.org/10.1609/aaai.v37i8.26192>
- [24] Zonghan Wu, Shirui Pan, Guodong Long, Jing Jiang, Xiaojun Chang, and Chengqi Zhang. 2020. Connecting the Dots: Multivariate Time Series Forecasting with Graph Neural Networks. In *KDD*. ACM, 753–763. <https://doi.org/10.1145/3394486.3403118>
- [25] Zonghan Wu, Shirui Pan, Guodong Long, Jing Jiang, and Chengqi Zhang. 2019. Graph WaveNet for Deep Spatial-Temporal Graph Modeling. In *IJCAI*. 1907–1913. <https://doi.org/10.24963/ijcai.2019/264>
- [26] Yaowen Ye, Lianghao Xia, and Chao Huang. 2023. Graph Masked Autoencoder for Sequential Recommendation. In *SIGIR*. 321–330. <https://doi.org/10.1145/3539618.3591692>
- [27] Jiaqi Zeng and Pengtao Xie. 2021. Contrastive self-supervised learning for graph classification. In *Proceedings of the AAAI conference on Artificial Intelligence*, Vol. 35. 10824–10832.
- [28] Chenhan Zhang, James Jian Qiao Yu, and Yi Liu. 2019. Spatial-Temporal Graph Attention Networks: A Deep Learning Approach for Traffic Forecasting. *IEEE Access* 7 (2019). <https://doi.org/10.1109/ACCESS.2019.2953888>
- [29] Richard Zhang, Phillip Isola, and Alexei A. Efros. 2016. Colorful Image Colorization. In *ECCV (Lecture Notes in Computer Science, Vol. 9907)*. 649–666. https://doi.org/10.1007/978-3-319-46487-9_40
- [30] Chuanpan Zheng, Xiaoliang Fan, Cheng Wang, and Jianzhong Qi. 2020. GMAN: A Graph Multi-Attention Network for Traffic Prediction. In *AAAI*. 1234–1241.

A DATASET DETAILS

Four widely used traffic datasets¹ are selected to evaluate the effectiveness of STMAE on the traffic forecasting task. These include:

- PEMS03 [19]: The dataset contains traffic flow data in the Bay Area. 307 sensors are used for data collection starting from 09/01/2018 to 12/01/2018.
- PEMS04 [7]: The dataset contains traffic flow data in the Bay Area. There are 307 sensors and the period of data ranges from 01/01/2018 to 02/28/2018.
- PEMS07 [19]: The dataset contains traffic flow information from California. The data is collected by 883 sensors from 05/01/2017 to 08/07/2017.
- PEMS08 [7]: The dataset contains traffic flow information collected from 170 sensors in the San Bernardino area from 07/01/2016 to 08/31/2016.

The number of variables (sensors) N , number of edges, the density of the predefined graph \mathcal{G} and the time range are summarized in table 3. We follow the practices in [14] to construct the predefined graphs that are necessary for DCRNN, that the adjacency matrix A is constructed by road-network distance using Gaussian thresholding [18]. Formally,

$$A_{uv} = \begin{cases} \exp\left(-\frac{\text{dist}(u,v)^2}{\sigma^2}\right), & \text{if } \text{dist}(u,v) \leq k \\ 0, & \text{otherwise,} \end{cases} \quad (9)$$

where $\text{dist}(u,v)$ denotes the road network distance between sensor u and v , σ denotes distance standard deviation, and $k = 0.1$ is the threshold. The training, validation, and testing dataset partition split is performed with a ratio of 6:2:2 for all four datasets, and the partition details are provided in table 4, where each instance represents a 5-minute traffic recording.

Table 3: Dataset statistics.

Datasets	#Sensors	#Edges	Density	Time Range
PEMS03	358	442	0.007	09/18 - 11/18
PEMS04	307	209	0.004	01/18 - 02/18
PEMS07	883	790	0.002	05/17 - 08/17
PEMS08	170	137	0.01	07/16 - 08/16

Table 4: Dataset partition details.

Datasets	#Training	#Validation	#Testing	#Instances
PEMS03	15,724	5,242	5,242	26,208
PEMS04	10,195	3,398	3,399	16,992
PEMS07	16,934	5,645	5,645	28,224
PEMS08	10,713	3,571	3,572	17,856

B BASE MODEL DETAILS

To study STMAE’s effectiveness in enhancing various backbones for traffic forecasting, three widely recognized spatial-temporal base models are used. These include:

- AGCRN [1]: a pioneer traffic forecasting framework which avoids relying on pre-defined graphs by learning the dependency graph dynamically from data. From the spatial side, AGCRN learns an adaptive graph on which graph convolution operates. Temporally, this adaptive graph convolution module is embedded in RNN to generate the state embeddings which are used for forecasting.
- DCRNN [13]: an early traffic forecasting framework incorporating the graph concept for spatial modeling. After graph construction, DCRNN learns spatial dependencies via bidirectional random walks on the graph, and the temporal correlations are modeled through RNNs with scheduled sampling. As a pioneer work, DCRNN is not as performative when compared to the other two base models.
- MTGNN [24]: a lightweight spatial-temporal forecasting framework. Similar to AGCRN, MTGNN also extracts relations among variables adaptively through a graph learning module. Differently, MTGNN relies on interleaved graph convolution and temporal convolution modules to capture the spatial-temporal dependencies within the data. Without utilizing recurrent structures, MTGNN is both more lightweight and computationally efficient compared with AGCRN and DCRNN.

The hyper-parameters of all three base models are used from their respective papers. For AGCRN, a two-layer RNN is used for encoding and one linear layer is used for prediction. The hidden dimension is 64, and the learning rate is 0.003. For DCRNN, both the encoder and decoder consist of two-layer RNNs with hidden dimension 64. With an initial learning rate of 0.01, scheduled sampling is employed with decay probability $\epsilon_i = \frac{\mu}{\mu + \exp(i/\mu)}$ at the i^{th} training step, where $\mu = 2000$ is the convergence rate. For MTGNN, three graph convolution modules and three temporal convolution modules are interleaved to learn spatial-temporal correlations with node embedding dimension of 40. The learning rate and gradient clipping is set to 0.001 and 5, respectively.

Besides STMAE, these base models are also integrated with STGCL [14], a contrastive learning-based spatial-temporal model enhancer. STGCL defines an auxiliary contrastive objective, which is jointly optimized alongside the main forecasting loss. This contrastive objective is calculated based on positive and negative samples, which are generated based on various data augmentation techniques guided by predefined heuristics. Following the original paper setup, we select input masking from {edge masking, input masking, temporal shifting, input smoothing} as base augmentation technique with ratio of 0.01 and a negative filtering threshold of 60 minutes. Based on paper recommendations, STGCL is trained with a two-layer multilayer perceptron with batch normalization layer as the contrastive projection head.

C PER-STEP RESULTS

In this section, we provide additional per-step MAE results, including (1) $STMAE_D$, DCRNN and $STGCL_D$ and (2) $STMAE_M$, MTGNN and $STGCL_M$ in figs. 7 and 8. The additional results further confirms STMAE’s ability in alleviating the performance degradation issue in spatial-temporal models with its generally enhanced performance over baselines.

¹<https://github.com/Davidham3/STSGCN/>

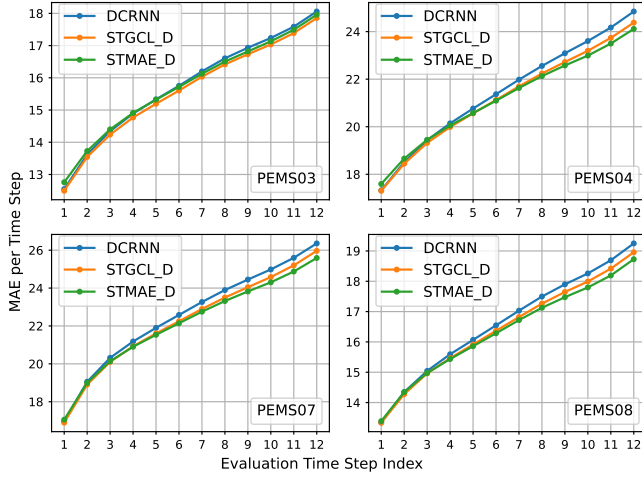


Figure 7: Per-step MAE results of $STMAE_D$ compared with its corresponding base model DCRNN and $STGCL_D$.

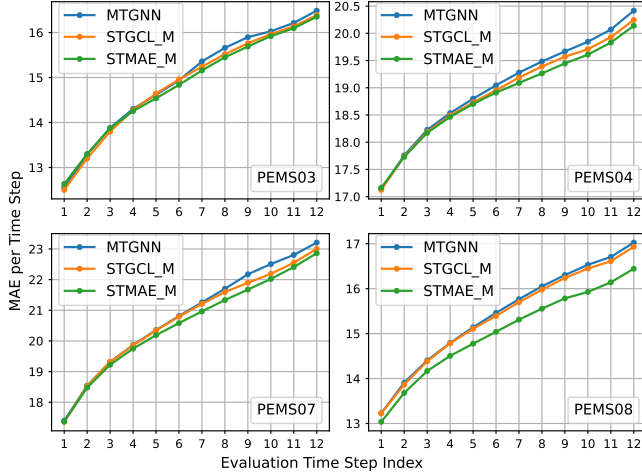


Figure 8: Per-step MAE results of $STMAE_M$ compared with its corresponding base model MTGNN and $STGCL_M$.

D ADDITIONAL VISUALIZATIONS

In this section, we provide additional qualitative visualizations in figs. 9, 10 and 12. To further demonstrate $STMAE$'s stability against data irregularities, we randomly select a subset of sensors and days from the PEMS03, PEMS04, PEMS07 and PEMS08 datasets, characterized by sudden traffic flow changes. We visualize one-hour-ahead predictions of $STMAE$ against the corresponding base models. From the areas highlighted by red rectangles, indicative of sudden flow changes, we can confirm that $STMAE$ is more robust to data irregularities, consistently outperforming the counterpart base models.

E ADDITIONAL ABLATION RESULTS

In this section, we include additional ablation results for evaluating $STMAE$'s overall design. Experimental results are presented in

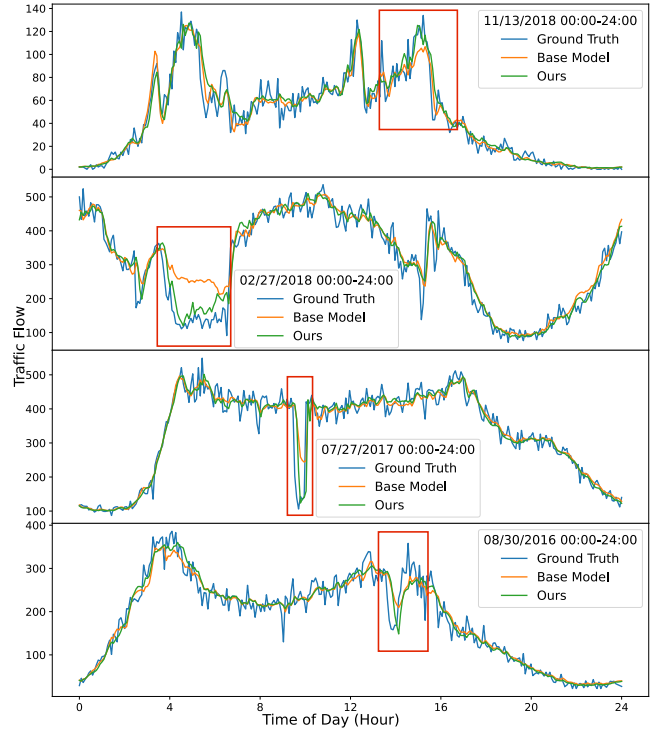


Figure 9: Visualizations of $STMAE_A$ and AGCRN one-hour-ahead predictions on snapshots from PEMS03, PEMS04, PEMS07 and PEMS08 test sets.

Table 5: Additional ablation results of $STMAE_A$ on PEMS03 and PEMS07. Best results are bolded and second bests are underlined.

Variant	PEMS03			PEMS07		
	MAE	MAPE	RMSE	MAE	MAPE	RMSE
AGCRN	15.47	15.26	27.06	20.64	8.80	<u>34.19</u>
$STMAE_{NT}$	15.30	15.26	<u>26.84</u>	20.52	8.81	34.28
$STMAE_{NS}$	15.27	15.30	27.05	20.42	8.63	34.29
$STMAE_U$	<u>15.25</u>	<u>15.12</u>	27.31	<u>20.38</u>	<u>8.50</u>	34.22
$STMAE_A$	15.09	14.72	26.61	20.13	8.53	33.79

table 5, with AGCRN serving as the backbone, while PEMS03 and PEMS07 are used as additional evaluation datasets. The results further underscores the advantages of our approach, where the advanced dual-masking strategy can create challenging pretext tasks for spatial-temporal models, thus improving their forecasting capacities.

F ADDITIONAL STABILITY STUDY RESULTS

We provide additional experimental results for $STMAE$ stability study in fig. 11, including visualizations of the learning curves for both the pretraining and fine-tuning stages of $STMAE_A$ on PEMS03 and PEMS07, alongside the learning curve for the AGCRN backbone.

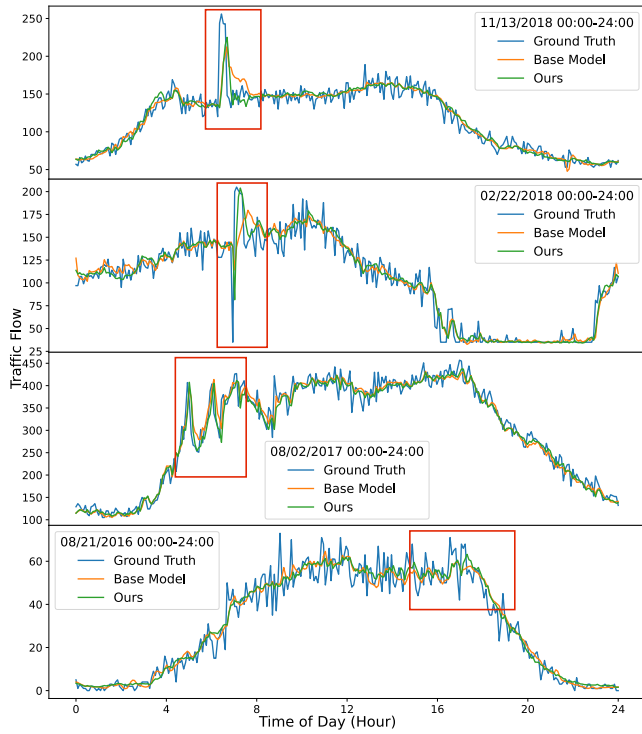


Figure 10: Visualizations of $STMAE_D$ and DCRNN one-hour-ahead predictions on snapshots from PEMS03, PEMS04, PEMS07 and PEMS08 test sets.

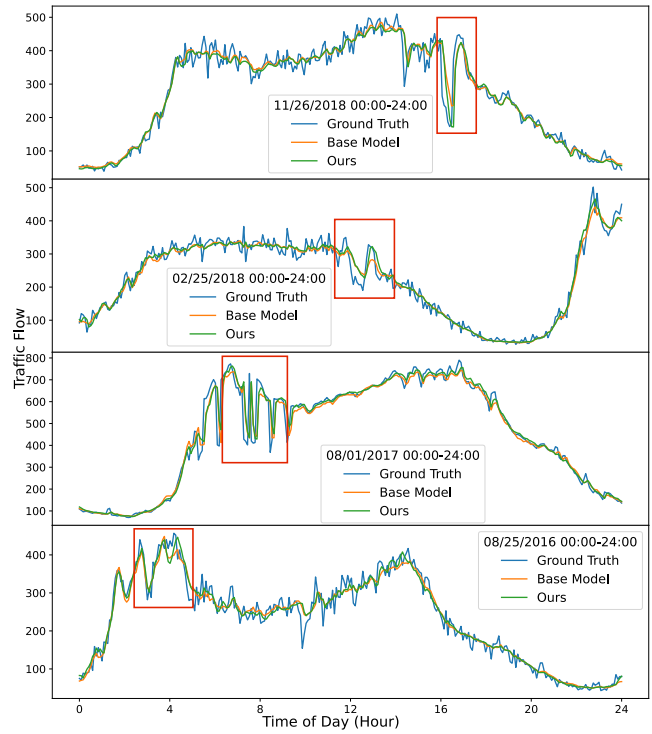


Figure 12: Visualizations of $STMAE_M$ and MTGNN one-hour-ahead predictions on snapshots from PEMS03, PEMS04, PEMS07 and PEMS08 test sets.

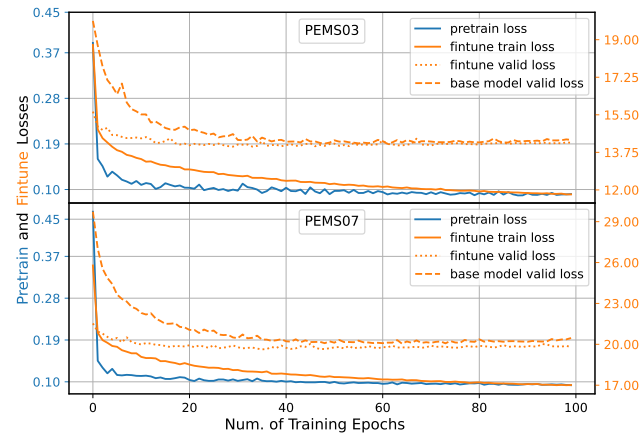


Figure 11: Additional training and validation processes of $STMAE_A$ and AGCRN on PEMS03 and PEMS07 datasets.

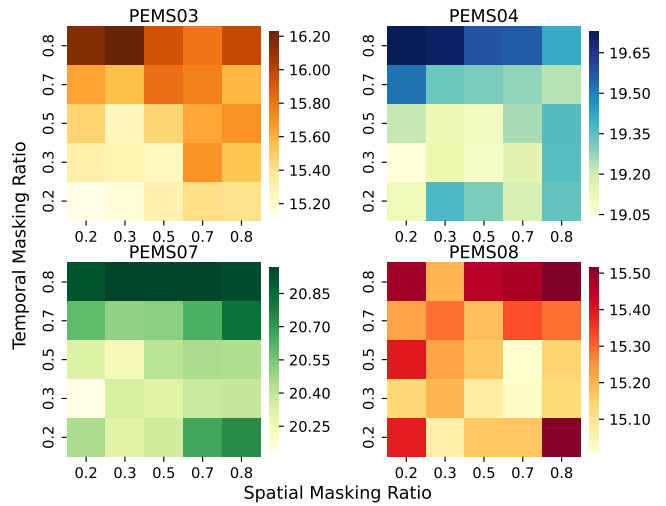


Figure 13: Masking ratio sensitivity analysis of $STMAE_A$ on PEMS03, PEMS04, PEMS07 and PEMS08. The values denote the MAE metric. Lighter is better.

G ADDITIONAL MASKING RATIO RESULTS

In this section, we include additional results for studying STMAE’s sensitivity to the spatial and temporal masking ratios. As mentioned in the main paper, we explore the impact of varying these ratios from 20% to 80% when coupling STMAE with AGCRN, and experimental results for all four datasets: PEMS03, PEMS04, PEMS07 and PEMS08 are shown in fig. 13, where the values indicate test set

MAE performance. From the heatmaps, we draw the same conclusion that STMAE exhibits optimal performance when the temporal masking ratio is around 20% to 30% for all datasets. On the other hand, from the spatial perspective, STMAE performs the best with a spatial masking ratio of 70% for PEMS08, while for other datasets, 20% to 30% is a more favorable choice. We attribute this difference to the greater physical structural density of PEMS08 as shown in table 3.